

## Accepted Manuscript

Experimental evidence for the interaction of C-60 fullerene with lipid vesicle membranes

Jernej Zupanc, Damjana Drobne, Barbara Drasler, Janez Valant, Ales Iglic, Veronika Kralj-Iglic, Darko Makovec, Michael Rappolt, Barbara Sartori, Ksenija Kogej

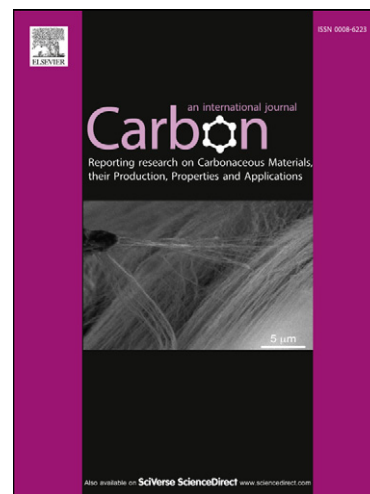
PII: S0008-6223(11)00860-8  
DOI: [10.1016/j.carbon.2011.10.030](https://doi.org/10.1016/j.carbon.2011.10.030)  
Reference: CARBON 6898

To appear in: *Carbon*

Received Date: 18 August 2011  
Accepted Date: 18 October 2011

Please cite this article as: Zupanc, J., Drobne, D., Drasler, B., Valant, J., Iglic, A., Kralj-Iglic, V., Makovec, D., Rappolt, M., Sartori, B., Kogej, K., Experimental evidence for the interaction of C-60 fullerene with lipid vesicle membranes, *Carbon* (2011), doi: [10.1016/j.carbon.2011.10.030](https://doi.org/10.1016/j.carbon.2011.10.030)

This is a PDF file of an unedited manuscript that has been accepted for publication. As a service to our customers we are providing this early version of the manuscript. The manuscript will undergo copyediting, typesetting, and review of the resulting proof before it is published in its final form. Please note that during the production process errors may be discovered which could affect the content, and all legal disclaimers that apply to the journal pertain.



**Experimental evidence for the interaction of C-60  
fullerene with lipid vesicle membranes**

*Jernej Zupanc*<sup>1</sup>, *Damjana Drobne*<sup>2,3,4,\*</sup>, *Barbara Drasler*<sup>3</sup>, *Janez Valant*<sup>2</sup>, *Ales Iglic*<sup>5</sup>, *Veronika Kralj-Iglic*<sup>6</sup>, *Darko Makovec*<sup>4,7</sup>,  
*Michael Rappolt*<sup>8</sup>, *Barbara Sartori*<sup>8</sup>, *Ksenija Kogej*<sup>9</sup>

<sup>1</sup>Faculty of Computer and Information Science, University of Ljubljana

Trzaska 25, SI-1000 Ljubljana, Slovenia

<sup>2</sup>Biotechnical Faculty, Department of Biology, University of Ljubljana

Vecna pot 111, SI-1000 Ljubljana, Slovenia

<sup>3</sup>Centre of Excellence in Advanced Materials and Technologies for the Future (CO NAMASTE)

Jamova 39, SI-1000 Ljubljana, Slovenia

<sup>4</sup> Centre of Excellence in Nanoscience and Nanotechnology (CO Nanocenter)

Jamova 39, SI-1000 Ljubljana, Slovenia

\*Corresponding author. Fax: +386 1 257 3390.  
E-Mail address: damjana.drobne@bf.uni-lj.si (D. Drobne)

<sup>5</sup> Laboratory of Biophysics, Faculty of Electrical Engineering,  
University of Ljubljana  
Trzaska 25, SI-1000 Ljubljana, Slovenia

<sup>6</sup> Laboratory of Clinical Biophysics, Faculty of Medicine,  
University of Ljubljana  
Lipiceva 2, SI-1000 Ljubljana, Slovenia

<sup>7</sup>Institute Jozef Stefan  
Jamova 39, SI-1000 Ljubljana

<sup>8</sup> Institute of Biophysics and Nanosystems Research, Austrian  
Academy of Science  
c/o Sincrotrone Trieste, 34149 Basovizza, Italy

<sup>9</sup> Department of Chemistry and Biochemistry  
Faculty of Chemistry and Chemical Technology, University of  
Ljubljana  
PO Box 537, SI-1000, Ljubljana, Slovenia

**Abstract**

There are some molecular dynamic simulations but a paucity of experimental evidence of the effects of C-60 fullerene on lipid bilayers. The aim of this study is to assess the potential for disruption of the lipid bilayer by C-60 suspended in water. We selected a C-60 suspension that has previously been shown to provoke cell membrane destabilisation *in vivo*. Electromobility measurements show significant negative surface charge on the C-60 nanoparticles suspended in a glucose solution and a zeta potential of -26 mV. The prevalent C-60 clusters have hydrodynamic radii of approximately 2 nm. Phase contrast microscopy and computer aided image analysis results show that C-60 causes shape transformations and rupture of unilamellar phospholipid vesicles, indicative of changes in their average mean curvature. Small-angle X-ray scattering reveals that C-60 provokes disruptions of external membranes of multilamellar vesicles only after freeze and thaw cycles. Here, the liposomes undergo breakage and annealing steps which increase the probability for fullerenes to insert into the MLVs. Our experimental findings confirm the potential of C-60 to reconstruct lipids in biological membranes. This research enhances our understanding of the impact of engineered nanoparticles on cell membranes.

## 1. Introduction

Applications of C-60 fullerenes have been attracting increasing attention in different fields of research since their discovery in 1985 [1]. Upon exposure to water C-60 nanoparticles can form stable, negatively charged aggregates [2]. They are extremely hydrophobic and essentially insoluble - the solubility of C-60 in water is below  $10^{-9}$  mg l<sup>-1</sup> [3]. Despite this, it has been reported that C-60 as an aggregate in the aqueous phase is more cytotoxic than functionally derivatized, water soluble fullerenes such as polyhydroxylated C-60 [3,4]. The interaction of an aqueous suspension of pristine C-60 with cells is an important phenomenon which can be used to define and limit the biological applications of C-60. Simple and reproducible model systems are needed to delineate the physical principles governing these complex interactions.

Artificial lipid membranes are suitable simplified substitutes for cell membranes. Studies on giant unilamellar vesicles (GUVs) are especially popular because they are comparable in size to cells and can be observed directly by optical microscopy [5]. Vesicle shapes are not static, but fluctuate around an average shape [6-9] and lipid vesicle shape behaviour reflects some general features of biological membranes [10,11]. The mean shape of a vesicle is

determined by the minimum free energy of its bilayer membrane [12,13] under specific conditions and the area and volume of a vesicle can be considered fixed at constant temperature and constant osmotic pressure [14]. Experimental studies and theoretical descriptions have provided evidence that different substances such as detergents [15,16], and proteins [17], and environmental conditions such as temperature [5] and magnetic or electric fields [18] provoke vesicle shape transformations.

In addition to conventional light microscopy investigations, a number of other approaches have recently been employed for the experimental studies of lipid vesicles. These include small angle X-ray scattering (SAXS) experiments which allow elucidation of the bilayer structure of unilamellar or multilamellar vesicles [19]. These experiments provide information on the bilayer thickness, inter-membrane distance, and area per lipid molecule, as well as the number of spatially correlated membranes in multilamellar vesicles (MLVs). The present study is focused mainly on the ordering and disordering effects of C-60 on MLVs comprised of unilamellar phospholipid vesicle bilayers.

Interactions between nanoparticles and biological membranes that have been studied involve C-60 and its derivatives [20]. These interactions are studied either by computer simulation studies or

by experimental approach. Computer simulation studies suggest that C-60 may provoke formation of holes and pores in membranes, and induce changes in the structural and elastic properties of the lipid bilayer, and in its phase transformations [21, 22, 23, 24, 25, 26].

Experimental studies supported the computer simulation studies on incorporation of C-60 into the lipid membranes leading to structural changes of phospholipid layers [27,28] and cell contraction [29].

Wong-Ekkabut et al. [30] reported a computer study that suggested permeation of a solid-like fullerene aggregate into the lipid bilayer was thermodynamically favoured and occurred on the microsecond timescale. They also concluded that high concentrations of fullerenes induced changes in the structural and elastic properties of the lipid bilayer, but the changes were not significant enough to mechanically damage the membrane. They suggested that mechanical damage was an unlikely mechanism for membrane disruption and fullerene toxicity.

In vitro studies with different cell cultures have confirmed the potential of C-60 to affect cell membranes. Sayes et al. [31]

explained that reactive oxygen species (ROS) are responsible for membrane damage and Kamat et al. [32] attributed membrane damage to lipid peroxidation, damage to proteins and loss of the membrane-bound enzymes. Solomadin et al. [33] reported that water-soluble fullerene C-60 caused lysis of human and rat erythrocytes and Isakovic et al. [34] reported the strong pro-oxidant capacity of pure fullerene suspension (nano-C-60) which is responsible for the rapid cell necrosis. Yang et al. [35] also provided evidence that fullerene derivatives might induce damage to biological membranes, but they reported that prior to leakage of the cytoplasmic membrane, a transient increase in calcium occurred due to influx of calcium from the culture medium.

It has often been reported that C-60 in a water suspension may generate reactive oxygen species. Li et al. [36] provided experimental evidence for lipid peroxidation in small and large phospholipid unilamellar vesicles induced by water-soluble free radical sources generated by C-60. Similar results were reported by Guldi and Prato [37] who suggested that the high electron affinity of C-60 coupled with available oxygen and water resulted in generation of radicals. Foley et al. [38] also found these materials can generate oxygen radicals, including superoxide anion which is primarily responsible for peroxidation of the lipid bilayer. In contrast, results published by Lee et al. [39] suggested that nano-C-

60 in water might not trigger ROS production. They speculated that C-60 might produce ROS only in specific environments, for example within a lipid bilayer, a condition similar to that experienced by surfactant micelles.

The aim of our work was to assess the potential of C-60 to affect the phase of the phospholipids in the cell membrane. We used the same C-60 water suspension in the same concentration range we had previously observed to provoke cell membrane destabilisation in vivo [40] and hypothesised that if a C-60 water suspension affected the lipid component of a cell membrane, the artificial phospholipid vesicles would also be affected. We used phase contrast microscopy and computer aided image analysis to investigate morphological transformations and changes in abundance (bursting) of vesicles incubated for up to 120 min in a C-60 water suspension. In addition, SAXS was used to resolve structural details of multilamellar 1-palmitoyl-2-oleoyl-*sn*-glycero-3-phosphocholine (POPC) vesicles incubated with an aqueous suspension of C-60. The mode of interaction between C-60 and artificial lipid vesicles is discussed and the relevant data is compared to that obtained in vivo with the same C-60 suspensions.

## 2. Experimental

### 2.1 Chemicals

Synthetic POPC and cholesterol, obtained from Avanti Polar Lipids, Inc. (Alabaster, AL, USA) were dissolved in a mixture of  $\text{CHCl}_3$  (66%, v/v) and MeOH (33%, v/v). C-60 and sucrose were purchased from Sigma–Aldrich (Steinheim, Germany). A 0.3M aqueous sucrose solution was prepared using distilled water. Glucose solution (5%, for intravenous applications) was purchased from Krka, d.d. (Novo Mesto, Slovenia).

### 2.2 Nanoparticle suspensions

#### 2.2.1 Preparation of nanoparticle suspensions

A stock suspension of C-60 nanoparticles with concentration  $1 \text{ mg ml}^{-1}$  was prepared in distilled water. The suspension was bath-sonicated (20 kHz) for three days to obtain a stable dispersion of C-60 [41]. In the experiments below,  $5 \text{ }\mu\text{l}$  of water containing suspended nanoparticles was added to  $45 \text{ }\mu\text{l}$  of 5% glucose solution containing lipid vesicles.

#### 2.2.2 Characterization of nanoparticle suspensions

Characterisation of nanoparticles (primary characteristics of nanoparticles) and their suspensions (secondary characteristics of nanoparticles) were assessed by transmission electron microscopy (TEM), DLS (dynamic light scattering) and  $\zeta$ -potential measurements.

Specimens for TEM were prepared by drying the suspension of nanoparticles on a copper-grid-supported, perforated, transparent carbon foil at room temperature. TEM analysis was performed using a JEOL 2100 TEM (Tokyo, Japan) operated at 200 kV and equipped with an energy-dispersive X-ray spectrometer (EDX).

Dispersed nanoparticles were inspected by DLS using a 3D DLS-SLS spectrometer (LS Instruments, Fribourg, Switzerland). This enabled determination of the hydrodynamic radii of particles in extremely turbid suspensions by a so-called 3D cross-correlation technique that successfully tolerates multiple scattering of light. A HeNe laser operating at a wavelength of 632.8 nm was used as the light source and scattering was measured at an angle of 90°. In a DLS experiment, the time correlation function of the scattered light intensity,  $G_2(t)$ , was measured and from this, the distribution of the hydrodynamic radii,  $R_h$ , was obtained by CONTIN analysis (Schärtl 2007). The zeta potential of suspended C-60 nanoparticles was measured with ZetaPals (Brookhaven Instruments Corporation, Holtsville, NY, USA). The osmolarity of the C-60 water suspension was compared to that of distilled water (Vapor Pressure Osmometer K-7000, Berlin, Germany).

### 2.3 *Giant unilamellar vesicles*

#### 2.3.1 *Preparation of giant unilamellar vesicles*

GUVs were prepared by a modified method of electroformation [42] at room temperature from POPC (80%, v/v) and cholesterol (20%, v/v). The solution of the lipid mixture (40  $\mu$ l) was spread over two platinum electrodes and the solvent was allowed to evaporate in vacuum for 2 hours. The coated electrodes were then placed 4 mm apart in an electroformation chamber containing 2 ml of 0.3M sucrose solution. An alternating electric field of magnitude 5 V mm<sup>-1</sup> and frequency of 10 Hz was applied to the electrodes for 2 h. The magnitude and frequency of the alternating electric field was then gradually reduced at intervals of 15 min, first to 2.5 V mm<sup>-1</sup> and 5 Hz, then to 2.5 V mm<sup>-1</sup> and 2.5 Hz and finally to 1 V mm<sup>-1</sup> and 1 Hz. After the electroformation, 600  $\mu$ l of 0.3M sucrose solution containing electroformed GUVs was added to 1 ml of 0.3M glucose solution. The vesicles were left to sediment for approximately 24 h in vacuum at room temperature. Then the container was inverted twice, 100  $\mu$ l of the supernatant was removed and vesicles were taken from the bottom of the vial.

#### 2.3.2 *Giant unilamellar vesicle population experiment*

The vesicles were created in sucrose solution and rinsed with an equi-osmolar glucose solution. Prepared in this way, the intact membrane is not permeable to sugar molecules, and the content of

the vesicles, which is primarily sucrose, differs from the extravascular sucrose/glucose medium. As a result, the interior of the lipid vesicles appears to be darker than the surrounding medium in the micrographs, and is more easily distinguished from the background. A sucrose/glucose suspension droplet containing lipid vesicles (45  $\mu$ l) was applied to an object glass and a strip of silicone gel was applied to the cover glass, surrounding two edges of the GUV droplet, acting as a spacer between the cover and object glass. Subsequently, a droplet of C-60 suspended in distilled water was added to the vesicles and silicon paste was applied to the remaining two edges of the cover glass to minimize evaporation (Fig. 1a). The vesicles gravitated to the bottom of the suspension within minutes (Fig. 1b).

Fig. 1 - (a) Scheme of the GUV population experiment. Lipid vesicle solution in the observation chamber, a recording area (P1) is selected and the suspension with the investigated additive is added. (b). Transverse section of the observation chamber and the lipid vesicle suspension. A majority of the vesicles are in the same focal plane, at the bottom of the observation chamber. (c) The observation chamber under the microscope, with the direction of recording. These schemes are not to scale.

One-dimensional tracks of the specimen were recorded 1, 10, 100, and 120 min after the vesicle population was applied to the object glass at the start of the experiment. The nanoparticles were added between the first and second recordings, approximately 5 min after the start of the experiment. In every recording of a 1-dimensional track, 15 micrographs were acquired at 400x magnification, each covering a field of 200 x 150  $\mu\text{m}$  with a resolution of 768 x 576 pixels (Fig. 1c). In this way, a subsample of the population was captured in which all vesicles of a single track were at approximately the same distance from the place on the object glass, where the nanoparticle suspension was added. A Nikon Eclipse TE2000-S inverted phase contrast light microscope attached to a Sony XC-77 CE CCD video camera module was used as the imaging system. The vesicles in the micrographs were manually labeled with the use of our “Shape Segmenter” plug-in for ImageJ [42]. Spherical vesicles, pears, pearls and tubular vesicles were each assigned a separate color, and data on separate vesicle types was extracted using Matlab 2009b (Mathworks, Natick, MA, USA). Excel 2007 (Microsoft Corp., Redmond, WA, USA) was used for statistical analysis.

## 2.4 Multilamellar vesicles

### 2.4.1 Preparation of MLVs

MLVs of POPC were prepared by dispersing weighed amounts of lipid powder in either (i) pure distilled water or (ii) water containing 1 mg ml<sup>-1</sup> of C-60 sample. The final concentration of MLVs was 10%. The dispersions were kept at room temperature for 1 h in a sealed vial and then each dispersion was vortexed for 10 min. To increase the probability of fullerene insertion into the MLVs, one particular sample with fullerene was additionally subjected to 10 freeze and thaw cycles, *i.e.* the lipid dispersion was shock-frozen in liquid nitrogen, then thawed for 5 min reaching a final temperature of 60 °C. After 10 such cycles, the dispersion was vigorously vortexed for 1-2 min.

### 2.4.2 X-ray measurements and analysis of MLVs

SAXS experiments were performed with a small and wide angle X-ray scattering camera with Kratky collimation (SWAXS, Hecus X-ray Systems GmbH, Graz, Austria) [43] mounted on a sealed-tube generator (Philips PW 1729, Philips, Holland) operating at 2 kW. Cu-K $\alpha$  radiation ( $\lambda=0.154$  nm) was selected using a tungsten filter. A linear one-dimensional position-sensitive detector (PSD 50-M, Hecus X-ray Systems GmbH, Graz, Austria) covered the  $q$ -range of interest ( $q = 4 \sin^{-1} \frac{\lambda}{2d}$ , where  $\lambda$  is the wavelength and  $2\theta$  is the scattering angle) from 0.2 to 6 nm<sup>-1</sup>. Silver behenate, CH<sub>3</sub>-

(CH<sub>2</sub>)<sub>20</sub>-COOAg with a  $d$  spacing value of 5.84 nm, was used as a standard to calibrate the angular scale of the measured intensity [44]. The MLV dispersions were transferred to a 1.5 mm capillary and measured at room temperature. The exposure time was set to 30 min. The background from water and the capillary was subtracted.

For analysis of the small angle diffraction pattern, the first order Bragg peaks were fitted with Lorentzian distributions using Origin 5.0 software (OriginLab, Northampton, MA, USA). The full width at half maximum (FWHM),  $\Delta q_{exp}$ , was used to estimate the average number  $N$ , of positionally correlated bilayers in the MLVs. The measured  $\Delta q_{exp}$  was corrected for the instrumental beam width,  $\Delta q_0$ , according to the relation  $\Delta q \approx \sqrt{(\Delta q_{exp})^2 - (\Delta q_0)^2}$  where  $\Delta q_0 = 0.082 \text{ nm}^{-1}$ . Finally,  $N$  was estimated by Scherrer's equation [45]:

$$\Delta q (FWHM) \approx \frac{2\pi}{N \cdot d} = \frac{q_c}{N}, \quad (1)$$

where  $q_c$  is the centre of the first order diffraction peak.

### 3. Results

#### 3.1 Characteristics of nanoparticle suspensions

TEM analysis showed the nanoparticles ( $100 \mu\text{g ml}^{-1}$ ) to range in size from approximately 15 nm to 50 nm. The primary nanoparticles form clusters and aggregates, which are fairly

monodisperse in size (Fig. 2). Electron diffraction experiments showed the amorphous nature of the nanoparticles.

Fig. 2 - TEM micrograph of C-60 clusters in an aggregated state ( $100 \mu\text{g ml}^{-1}$ ). The image shows nanoparticles which form agglomerates.

As expected, EDX analysis of C-60 detected only carbon.

The correlation function obtained for a suspension of C-60 in a glucose solution is shown in Fig. 3a together with the corresponding distribution of the hydrodynamic radii ( $R_h$ ). Two peaks are seen in the intensity distribution function: the first has an  $R_h$  value of 155 nm and the other a considerably larger  $R_h$  ( $> 1000$  nm), denoting that C-60 molecules are present in very large clusters. An individual C-60 molecule is 0.706 nm in diameter. However, these large particles, which contribute significantly to the intensity of the scattered light, can no longer be seen in the number (or mass) weighted distributions (Fig. 3b). Fig. 3b shows that the prevailing species in these suspensions are considerably smaller particles with  $R_h \sim 2$  nm, which still suggests some aggregated form of C-60 molecules. The eventual presence of individual C-60 spheres cannot be confirmed by DLS, since they are too small to be detected by this technique. Electromobility

measurements showed significant negative surface charge on the C-60 nanoparticles suspended in the glucose solution resulting in a  $\zeta$ -potential of -26 mV.

Fig. 3 - (a) The normalized correlation function of the scattered light intensity,  $G_2(t)$ , at  $90^\circ$  (open circles) and the corresponding intensity weighted distribution function of the hydrodynamic radii,  $R_h$ , obtained from the CONTIN analysis of  $G_2(t)$  for C-60 suspension in glucose (Inset). The solid red line shows the multiexponential fit of the measured correlation function. (b) The corresponding mass and number weighted distributions of C-60 ( $100 \mu\text{g ml}^{-1}$ ). A general designation  $W_i$  is used for the fraction of species in these distributions.

### 3.2 *Giant unilamellar vesicle population exposed to C-60*

#### 3.2.1 *GUVs in distilled water*

After the vesicles had been incubated in distilled water for 10 min, their average number was not reduced as could have occurred due to osmotic stress. On the contrary, there was a slight increase in the quantity of vesicles which is ascribed to their negative buoyancy. This results in collection of vesicles in the focal plane, at the bottom of the chamber, in the first minutes of incubation [46]. Moreover, there were no differences in osmolarity between

distilled water and the suspension of C-60 in distilled water. We take this as evidence that distilled water has no effect on the abundance of vesicles. Therefore in the main experiment nanoparticles were suspended in distilled water.

### 3.2.2 *Effect of C-60 on GUV quantity*

In Fig. 4, it can be seen that the quantity of segmented vesicles before incubation with C-60 was similar in all three independent experiments (each time a control population and a C-60 exposed population were compared). In the control population, the quantity of segmented vesicles increased in the first 10 minutes after they had been placed on the object glass which is explained as a result of their negative buoyancy. At subsequent observation times, no differences in the quantity of vesicles in the control populations were detected. This pattern was observed in each of the three experiments.

Fig. 4 - Quantities of segmented vesicles after different periods of incubation. Less than five minutes after addition of C-60 to the vesicle population, a decrease in the number of vesicles in the population can be seen. Each box plot represents three experiments. Each line in the box (upper, lower and medium) corresponds to a value obtained in an individual experiment. A

small rectangle inside the box shows the mean quantity of vesicles obtained as an average of the three experiments.

In the C-60-incubated vesicle population, significant reduction of the vesicle quantity was evident soon after the addition of nanoparticles. We found that two thirds of the vesicles ruptured within minutes of incubation. Prolonged duration of exposure to C-60 water suspension did not further decrease the abundance of vesicles.

### 3.2.3 Vesicle morphology

Fig. 5 - (a) Spherical GUVs. (b-d) GUVs shaped as pears. In the whole population 188 such pears were identified, i.e. approximately 6% of the total vesicle population.

The computational approach used in our study revealed that 94% (2973 out of 3121) of the vesicles were spherical. Approximately 6% of the vesicles were non-spherical, predominantly pears (Fig. 5), but also pearls, and occasionally tubes. In the control populations, a slight increase in the quantity of pears was observed 10 minutes after placing vesicles on the object glass. Also here we explain this as the effect of sedimentation. In the populations exposed to C-60 we detected a decline in the number of pears immediately after addition of nanoparticles (Fig. 6).

Fig. 6 - Portion of pears per 1000 vesicles as a function of time.

Each box presents combined data from three experiments.

Over time, the quantity of pears in the C-60 exposed population on average remained lower than in the control population (Fig. 6).

### 3.3 *MLVs exposed to C-60*

In Fig. 7 the background subtracted SAXS pattern of POPC MLVs in the absence (black) and presence (red and blue) of C-60 in excess water are displayed. When MLV dispersions containing fullerene were prepared by the standard methods described above, the vesicles were slightly stabilized as indicated by the improved quasi-long range order in the lattice. This can be readily seen in the SAXS patterns shown in Fig. 7: a third order diffraction peak (circled in red) appears at  $q \sim 3 \text{ nm}^{-1}$  and closer analysis of the first order Bragg peak confirms this observation.

Fig. 7 - SAXS pattern of POPC MLVs at room temperature. (i) POPC MLVs in water, (ii) POPC MLVs in the presence of fullerenes, and (iii) POPC MLVs with fullerenes after 10 cycles of freeze and thaw.

The average number  $N$ , of positionally correlated bilayers increases from approximately 10 to 30, and at the same time the lattice repeat distance decreases by 0.1-0.2 nm (Table 1).

Table 1: Structural parameters of different POPC MLVs.

However, when the MLV dispersion is additionally treated with shock-freeze and thaw cycles, the situation is reversed. In this case, the vesicles underwent breakage and annealing steps, and thus the probability that fullerenes could insert into the MLVs was increased. The upper (blue) SAXS pattern shows a stronger lattice disorder ( $N \sim 6$ ), although the lattice parameter,  $d$ , remains unaltered (Table 1).

#### 4. Discussion

This study provides experimental evidence that a suspension of C-60 in water causes rupture of POPC lipid vesicles (GUVs) and changes of vesicle shapes. No change in the GUVs halo brightness during C-60 incubation was observed suggesting that membrane permeability was not affected significantly before the rupture [47]. Disturbances of MLVs due to the C-60 were demonstrated only when the system was subjected to shock-freeze and thaw cycles. In this circumstance the C-60 probably enters the MLVs where it begins to disturb the lamellar lattice order. In this case, the

probability for fullerenes to insert into the layers of MLVs is increased as liposomes undergo breakage and annealing steps. In the absence of this rigorous freeze and thaw treatment the MLVs are stabilized by the addition of C-60. The explanation for this observation may be that adherent fullerenes are not readily able to penetrate the MLVs and they are likely to remain adhered to the outside of the vesicles, possibly contributing to their mechanical stabilization. Interaction between fullerenes and lipid membranes may lead also to changes in membrane elasticity and membrane fluidity. Salonen et al. [29] reported that C-70-GA complexes translocate across the membranes of HT-29 cells and enter nuclear membranes. Confocal imaging further reveals the real-time uptake of C-70-GA and the consequent contraction of the cell membranes. This contraction is attributed to the aggregation of nanoparticles into microsized particles promoted by cell surfaces.

The SAXS pattern suggests C-60 probably disrupts the liposomes to some extent, at least locally (Fig. 7). The loss of long range order can in principle be caused by two different mechanisms: (i) With 100 to 200 nm the C-60 agglomerates are far too big to be incorporated into the bilayer core (note that the bilayers thickness is about 4-5 nm only [48]), but they may locally perturb the membrane stacking in the MLVs when accumulating in the inter-membrane region where the thickness of the water layer at

equilibrium is about 1.8 nm; (ii) alternatively, it is possible that single C-60 molecules begin to adsorb into the hydrophobic core of the bilayers where they induce a decrease in bilayer rigidity, giving rise to stronger Helfrich undulations of the bilayers (*i.e.* increasing the repulsive membrane forces).

Data on aggregation patterns of C-60 in an aqueous suspension show different sizes of aggregates. Some were around 155 nm and others were considerably larger ( $R_h > 1000$  nm). However, the predominant species in these aqueous suspensions are considerably smaller particles with  $R_h \sim 2$  nm, still suggesting some aggregated form of C-60 molecules.

A possible explanation for the rupture of vesicles could be the osmotic shock caused by adding the suspension with lower osmolarity than the one in which the vesicles had originally been incubated but this possibility was excluded experimentally by measuring osmolarity of C-60 water suspensions and distilled water – there were no changes among those values. The rupture of vesicles incubated in C-60 water suspensions can be explained by the effect of nanoparticles on the effective average mean curvature of the bilayer membrane. This has the effect of driving the vesicles towards the limiting shape of extreme average mean curvature, *i.e.* spheres [49]. Since the membrane cannot resist further increase of

the average mean curvature it becomes stressed and finally ruptures [50, 51].

The experimental evidence provided in our study on the destruction of membranes by C-60 is consistent with computer simulations and experimental studies which report the potential of C-60 to disrupt lipid membranes leading to compromised permeability or membrane holes and pores [22-25, 30].

Shape transformations of lipid vesicles by nanoparticles were also described by Yu and Granick [18]. In the case when the nanoparticles were encapsulated inside the vesicles solely they [18] reported the formation of protrusions and growth of tubes from parent vesicle and finally the transformation of the tubular protrusions into pearls.

Subsequent addition of nanoparticles in the outer solution induced the reverse process, i.e. the shrinking of the vesicle tubular protrusions. No shape changes occurred when the particles were distributed only in the outer solution or when the concentration of the particles outside and inside the vesicles was the same [18]. It was suggested that adsorption of cationic nanoparticles on the zwitterionic headgroups of the lipids in the inner lipid layer induce the increase of the area per lipid [18,52]. The consequent

disturbance in the membrane may then result in the time dependent increase of the membrane spontaneous curvature (for example due to time dependent increase between the surface areas of the outer and the inner leaflet of the membrane bilayer) which may be a possible driving mechanism of the growth of thick tubular protrusions as observed by Yu and Granick [18].

Our results support the mechanism suggested by Yu and Granick [18]. Namely, the adsorption of anionic C-60 particles to the outer dipolar surface of the lipid vesicles decrease the area per zwitterionic lipid [52] which may then induce the time dependent change of the membrane spontaneous curvature leading to the time dependent vesicle shape transformation as shown in Fig.6. The time dependent shape transformation towards the limiting shapes composed of spherical membrane parts (spherical parent vesicle with endo or exo daughter vesicles [50,51]) finally ends with the rupture of the vesicle membrane when the membrane curvature cannot adapt anymore and the excessive membrane stress due to unfavourable spontaneous curvature can be released only by the rupture of the vesicle membrane which may include also the holes and pores formation [50,51].

There have been extensive studies of the interactions of lipid membranes with different exogenous species including nanoparticles. The binding efficiency of C-60 to lipid membranes or bilayers is very limited due to the strong aggregation behaviour of fullerenes. We confirmed this by SAXS, where disturbances of MLVs were observed only subsequent to shock-freeze and thaw cycles. The membrane stacks in the MLVs were disturbed by C-60 in only those cases and this was probably due to steric hindrance of aggregated fullerenes with its possible effects on the membrane rigidity. Without this vigorous freeze and thaw sample preparation, fullerenes were excluded from the MLVs. It is possible that fullerenes that simply adhere to the MLVs contribute to the mechanical stabilization of the MLVs.

Our SAXS data support the conclusion that C-60 in water suspension does not generate reactive oxygen species, because disruption of external membranes was evident only after freezing and thawing of vesicles mixed with the C-60 water suspension. If lipid peroxidation was a major reason for the damage to the membrane, the membrane would be affected without the “freezing and thawing” sample preparation.

The data on unilamellar and multilamellar vesicles incubated in C-60 water suspension support the hypothesis that solely C-60 may reconstruct lipids in lipid membranes [52,53]. Oxidative damage

may be a secondary event, but not necessarily the initial and sole mechanism of C-60 nanotoxicity.

In this study we used the same aqueous suspension of C-60 particles in the same concentration range as those known to cause in vivo cell membrane destabilisation [40]. By combining in vivo data with data on lipid vesicles we confirmed that C-60 water suspension has a potential to reconstruct lipids in a biological membrane as suggested by Dawson et al. [53]. This mechanism precedes the lipid peroxidation which had hitherto been supposed to be the initial mechanism of C-60 nanotoxicity [52,54].

## 5. Conclusions

- 1) C-60 aggregates in aqueous suspension include some very large aggregates ( $R_h \sim 155$  nm or  $R_h > 1000$  nm) but the predominant species in the suspensions have  $R_h \sim 2$  nm.
- 2) C-60 water suspension causes changes of the average mean curvature of the lipid membrane leading to the rupture of POPC vesicles.
- 3) Incubation of POPC vesicles in a suspension of C-60 ( $100 \mu\text{g ml}^{-1}$ ) causes rupture of approximately  $2/3$  of the vesicles within 10 minutes.
- 4) Disturbances of the lattice order of MLVs due to the incorporation of C-60 were observed, but only after the dispersions had been subjected to vigorous freeze and thaw cycles.

5) C-60 affects lipid membranes independent of lipid peroxidation. This was confirmed by MLVs which were not destroyed unless samples were treated with shock-freeze and thaw cycles. Our results suggest that lipid peroxidation is a step in the cascade of events involved in cytotoxicity and not the initial event.

6) The agreement of data on the destruction potential of C-60 on POPC vesicles and their effect on membrane disruption in vivo [40] confirms the capability of C-60 to destabilise cell membranes in vivo by interacting with the membrane lipids.

**Acknowledgements**

The Slovenian Research Agency supported part of this work under grants J1—9475, P1—0184 and P1-0201. We would like to thank G.W.A. Milne for editorial assistance.

**References**

[1] dos Santos LJ, Rocha GP, Alves RB, de Freitas RP. Fullerene C-60: Chemistry and Applications. *Quim Nova* 2010;33(3):680-93.

[2] Lyon DY, Adams LK, Falkner JC, Alvarez PJJ. Antibacterial activity of fullerene water suspensions: Effects of preparation method and particle size. *Environ Sci Technol* 2006; 15;40(14):4360-6.

[3] Ruoff RS, Tse DS, Malhotra R, Lorents DC. Solubility of C-60 in a Variety of Solvents. *J Phys Chem* 1993;97(13):3379-83.

[4] Heymann D. Solubility of fullerenes C-60 and C-70 in seven normal alcohols and their deduced solubility in water. *Fullerene Sci Technol* 1996;4(3):509-15.

[5] Kas J, Sackmann E. Shape Transitions and Shape Stability of Giant Phospholipid-Vesicles in Pure Water Induced by Area-to-Volume Changes. *Biophys J* 1991;60(4):825-44.

[6] Bivas I, Meleard P, Mircheva I, Bothorel P. Thermal shape fluctuations of a quasi spherical lipid vesicle when the mutual

displacements of its monolayers are taken into account. *Colloids Surf, A* 1999;157(1-3):21-33.

[7] Genova J, Zheliaskova A, Mitov MD. The influence of sucrose on the elasticity of SOPC lipid membrane studied by the analysis of thermally induced shape fluctuations. *Colloids Surf, A* 2006;282:420-2.

[8] Genova J, Zheliaskova A, Vitkova V, Mitov MD. Stroboscopic illumination study of the dynamics of fluctuating vesicles. *J Optoelectron Adv Mater* 2009;11(9):1222-5.

[9] Kralj-Iglic V, Gomisek G, Majhenc J, Arrigler V, Svetina S. Myelin-like protrusions of giant phospholipid vesicles prepared by electroformation. *Colloids Surf, A* 2001;181(1-3):315-8.

[10] Iglic A, Kralj-Iglic V. Effect of anisotropic properties of membrane constituents on stable shapes of membrane bilayer structure. In: Tien HT, Ottova-Leitmannova A, editors. *Planar Lipid Bilayers (BLMs) and their Applications*. Amsterdam: Elsevier SPC; 2003:143-172.

[11] Bagatolli LA, Ipsen JH, Simonsen AC, Mouritsen OG. An outlook on organization of lipids in membranes: Searching for a realistic connection with the organization of biological membranes. *Prog Lipid Res* 2010;49(4):378-89.

[12] Helfrich W. Elastic Properties of Lipid Bilayers - Theory and Possible Experiments. *Z Naturforsch, C: J Biosci* 1973;28(11-1):693-703.

[13] Kralj-Iglic V, Babnik B, Gauger DR, May S, Iglic A. Quadrupolar ordering of phospholipid molecules in narrow necks of phospholipid vesicles. *J Stat Phys* 2006;125(3):727-52.

[14] Farge E, Devaux PF. Shape Changes of Giant Liposomes Induced by an Asymmetric Transmembrane Distribution of Phospholipids. *Biophys J* 1992;61(2):347-57.

[15] Mavcic B, Babnik B, Iglic A, Kanduser M, Slivnik T, Kralj-Iglic V. Shape transformation of giant phospholipid vesicles at high concentrations of C12E8. *Bioelectrochemistry* 2004;63(1-2):183-7.

[16] Vitkova V, Genova J, Meleard P. Influence of alamethicin on the passive water permeability of model lipid membranes and on the morphology of giant lipid vesicles. *J Mater Sci: Mater Electron* 2003;14(10-12):819-20.

[17] Urbanija J, Tomsic N, Lokar M, Ambrozic A, Cucnik S, Rozman B, et al. Coalescence of phospholipid membranes as a possible origin of anticoagulant effect of serum proteins. *Chem Phys Lipids* 2007;150(1):49-57.

[18] Yu Y, Granick S. Pearling of Lipid Vesicles Induced by Nanoparticles. *J Am Chem Soc* 2009;131(40):14158-9.

[19] Rappolt M, Di Gregorio GM, Almgren M, Amenitsch H, Pabst G, Laggner P, et al. Non-equilibrium formation of the cubic Pn3m phase in a monoolein/water system. *Europhys Lett* 2006;75(2):267-73.

[20] Monticelli L, Salonen E, Ke PC, Vattulainen I. Effects of carbon nanoparticles on lipid membranes: a molecular simulation perspective. *Soft Matter* 2009;5(22):4433-45.

[21] Chang R, Lee J. Dynamics of C(60) Molecules in Biological Membranes: Computer Simulation Studies. *B Korean Chem Soc* 2010; 31(11): 3195-3200.

[22] Leroueil PR, Hong SY, Mecke A, Baker JR, Orr BG, Holl MMB. Nanoparticle interaction with biological membranes: Does nanotechnology present a janus face? *Acc Chem Res* 2007;40(5):335-42.

[23] Ginzburg VV, Balijepailli S. Modeling the thermodynamics of the interaction of nanoparticles with cell membranes. *Nano Lett* 2007;7(12):3716-22.

[24] Qiao R, Roberts AP, Mount AS, Klaine SJ, Ke PC. Translocation of C-60 and its derivatives across a lipid bilayer. *Nano Lett* 2007;7(3):614-9.

- [25] Chang R, Violi A. Insights into the effect of combustion-generated carbon nanoparticles on biological membranes: A computer simulation study. *J Phys Chem B* 2006;110(10):5073-83.
- [26] Bedrov D, Smith GD, Davande H, Li LW. Passive transport of C-60 fullerenes through a lipid membrane: A molecular dynamics simulation study. *J Phys Chem B* 2008;112(7):2078-84.
- [27] Jeng U, Lin TL, Shin K, Hsu CH, Lee HY, Wu MH, et al. Lipophilic C-60-derivative-induced structural changes in phospholipid layers. *Physica B* 2003; 336(1-2):204-210.
- [28] Katsamenis OL, Bouropoulos N, Fatouros DG. Interaction of Fullerenes C(60) with Large Unilamellar Vesicles. *J Biomed Nanotechnol* 2009; 5(4): 416-420.
- [29] Salonen E, Lin S, Reid ML, Allegood M, Wang X, Rao AM. Real-Time Translocation of Fullerene Reveals Cell Contraction. *Small* 2008; 4(11):1986-1992.
- [30] Wong-Ekkabut J, Baoukina S, Triampo W, Tang IM, Tieleman DP, Monticelli L. Computer simulation study of fullerene translocation through lipid membranes. *Nat Nanotechnol* 2008;3(6):363-8.
- [31] Sayes CM, Fortner JD, Guo W, Lyon D, Boyd AM, Ausman KD, et al. The differential cytotoxicity of water-soluble fullerenes. *Nano Lett* 2004;4(10):1881-7.

- [32] Kamat JP, Devasagayam TPA, Priyadarsini KI, Mohan H. Reactive oxygen species mediated membrane damage induced by fullerene derivatives and its possible biological implications. *Toxicology* 2000;155(1-3):55-61.
- [33] Solomadin IN, Marov NV, Venediktova NI, Kosenko EA, Kaminsky YG. Toxic effect of A beta(25-35) and fullerene C-60 on erythrocytes. *Biol Bull* 2008;35(4):436-40.
- [34] Isakovic A, Markovic Z, Todorovic-Markovic B, Nikolic N, Vranjes-Djuric S, Mirkovic M, et al. Distinct cytotoxic mechanisms of pristine versus hydroxylated fullerene. *Toxicol Sci* 2006;91(1):173-83.
- [35] Yang XL, Chen L, Qiao X, Fan CH. Photo-induced damages of cytoplasmic and mitochondrial membranes by a [C-60] fullerene malonic acid derivative. *Int J Toxicol* 2007;26(3):197-201.
- [36] Li QT, Yee MH, Tan BK. Lipid peroxidation in small and large phospholipid unilamellar vesicles induced by water-soluble free radical sources. *Biochem Biophys Res Commun* 2000;273(1):72-6.
- [37] Guldi DM, Prato M. Excited-state properties of C-60 fullerene derivatives. *Acc Chem Res* 2000;33(10):695-703.
- [38] Foley S, Crowley C, Smaih M, Bonfils C, Erlanger BF, Seta P, et al. Cellular localisation of a water-soluble fullerene derivative. *Biochem Biophys Res Commun* 2002;294(1):116-9.

[39] Lee J, Fortner JD, Hughes JB, Kim JH. Photochemical production of reactive oxygen species by C-60 in the aqueous phase during UV irradiation. *Environ Sci Technol* 2007;41(7):2529-35.

[40] Valant J, Drobne D, Sepcic K, Jemec A, Kogej K, Kostanjsek R. Hazardous potential of manufactured nanoparticles identified by in vivo assay. *J Hazard Mater* 2009;171(1-3):160-5.

[41] Dhawan A, Taurozzi JS, Pandey AK, Shan WQ, Miller SM, Hashsham SA, et al. Stable colloidal dispersions of C-60 fullerenes in water: Evidence for genotoxicity. *Environ Sci Technol* 2006;40(23):7394-401.

[42] Zupanc J, Dobnikar A, Drobne D, Valant J, Erdogmus D, Bas E. Biological reactivity of nanoparticles: mosaics from optical microscopy videos of giant lipid vesicles. *J Biomed Opt* 2011;16(2).

[43] Laggner P, Mio H. Swax - a Dual-Detector Camera for Simultaneous Small-Angle and Wide-Angle X-Ray-Diffraction in Polymer and Liquid-Crystal Research. *Nucl Instrum Methods Phys Res Sect A* 1992;323(1-2):86-90.

[44] Huang TC, Toraya H, Blanton TN, Wu Y. X-Ray-Powder Diffraction Analysis of Silver Behenate, a Possible Low-Angle Diffraction Standard. *J Appl Crystallogr* 1993;26:180-4.

[45] Klug HP, Alexander LE. X-ray diffraction procedures: for polycrystalline and amorphous materials. 2nd ed. New York: John Wiley & Sons, Inc.; 1974.

[46] Dobereiner HG, Evans E, Kraus M, Seifert U, Wortis M. Mapping vesicle shapes into the phase diagram: A comparison of experiment and theory. *Physical Review E* 1997;55(4):4458-74.

[47] Ambrozic A, Cucnik S, Tomsic N, Urbanija J, Lokar M, Babnik B, et al. Interaction of giant phospholipid vesicles containing cardiolipin and cholesterol with beta 2-glycoprotein-I and anti-beta 2-glycoprotein-I antibodies. *Autoimmun Rev* 2006;6(1):10-5.

[48] Pabst G, Rappolt M, Amenitsch H, Laggner P. Structural information from multilamellar liposomes at full hydration: Full q-range fitting with high quality x-ray data. *Physical Review E* 2000;62(3):4000-9.

[49] Kralj-Iglic V, Iglic A, Hagerstrand H, Peterlin P. Stable tubular microexovesicles of the erythrocyte membrane induced by dimeric amphiphiles. *Physical Review E* 2000;61(4):4230-4.

[50] Babnik B, Miklavcic D, Kanduser M, Hagerstrand H, Kralj-Iglic V, Iglic A. Shape transformation and burst of giant POPC unilamellar liposomes modulated by non-ionic detergent C12E8. *Chem Phys Lipids* 2003;125(2):123-138.

[51]: Mavcic B, Babnik B, Igljic A, Kanduser M, Slivnik T, Kralj-  
Igljic V. Shape transformations of giant phospholipid vesicles at  
high concentrations of C12E8. *Bioelectrochemistry* 2004;63(1-  
2):83-187.

[52] Wang B, Zhang LF, Bae SC, Granick S. Nanoparticle-induced  
surface reconstruction of phospholipid membranes. *P Natl Acad  
Sci USA* 2008; 105(47): 18171-18175.

[53] Dawson KA, Salvati A, Lynch I. Nanoparticles reconstruct  
lipids. *Nat Nanotechnol* 2009;4(2):84-5.

[54] Sayes CM, Gobin AM, Ausman KD, Mendez J, West JL,  
Colvin VL. Nano-C-60 cytotoxicity is due to lipid peroxidation.  
*Biomaterials* 2005;26(36):7587-95.

**Figure caption:**

Fig.1 - (a) Scheme of the lipid vesicle population experiment.  
Lipid vesicle solution in the observation chamber, a recording area  
(P1) is selected and the suspension with the additive under  
investigation is added.

Fig.1 – (b) Transverse section of the observation chamber and the  
lipid vesicle suspension. A majority of the vesicles are in the same  
focal plane, at the bottom of the observation chamber.

Fig.1 - (c) The observation chamber under the microscope, with  
the direction of recording Y. These schemes are not to scale.

Fig.2 - TEM micrograph of C-60 clusters in an aggregated state ( $100 \mu\text{g ml}^{-1}$ ). The image shows nanoparticles, which form agglomerate.

Fig.3 - (a) The normalized correlation function of the scattered light intensity,  $G_2(t)$ , at  $90^\circ$  (open circles) and the corresponding intensity weighted distribution function of the hydrodynamic radii,  $R_h$ , obtained from the CONTIN analysis of  $G_2(t)$  for C-60 suspension in glucose (Inset). The solid red line shows the multiexponential fit of the measured correlation function.

Fig.3 - (b) The corresponding mass and number weighted distributions of C-60 ( $100 \mu\text{g ml}^{-1}$ ). A general designation  $W_i$  is used for the fraction of species in these distributions.

Fig.4 - Quantities of segmented vesicles after different periods of incubation. Less than five minutes after addition of C-60 to the nano population, a decrease in the number of vesicles in the population can be seen. Each box plot represents three experiments. Each line in the box (upper, lower and medium) corresponds to a value obtained in an individual experiment. A small rectangle inside the box shows the mean quantity of vesicles obtained as an average of the three experiments.

Fig.5 - (a) Spherical GUVs.

Fig.5 - (b-d) Pear-shaped GUVs. In the whole population 188 such pears were identified, i.e. approximately 6% of the total vesicle population.

Fig.6 - Portion of pears per 1000 vesicles as a function of time.

Each box presents combined data from three experiments.

Fig.7 - SAXS pattern of POPC MLVs at room temperature. (i) POPC MLVs in water, (ii) POPC MLVs in the presence of fullerenes, and (iii) POPC MLVs with fullerenes after 10 cycles of freeze and thaw.

Fig 1

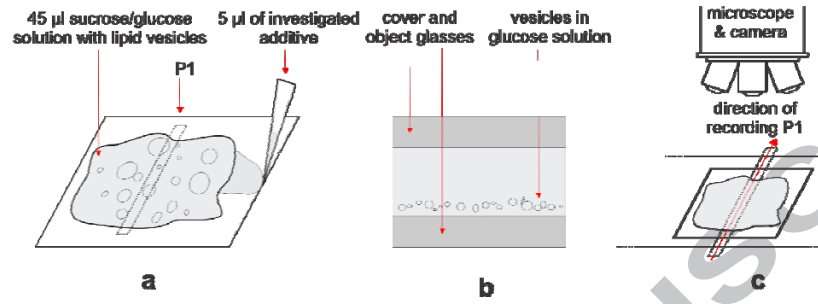


Fig 2

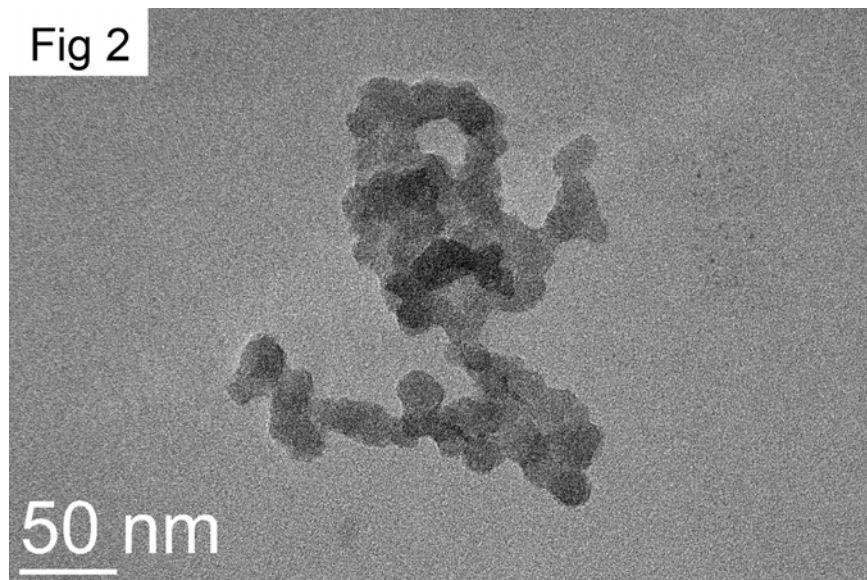


Fig 3a

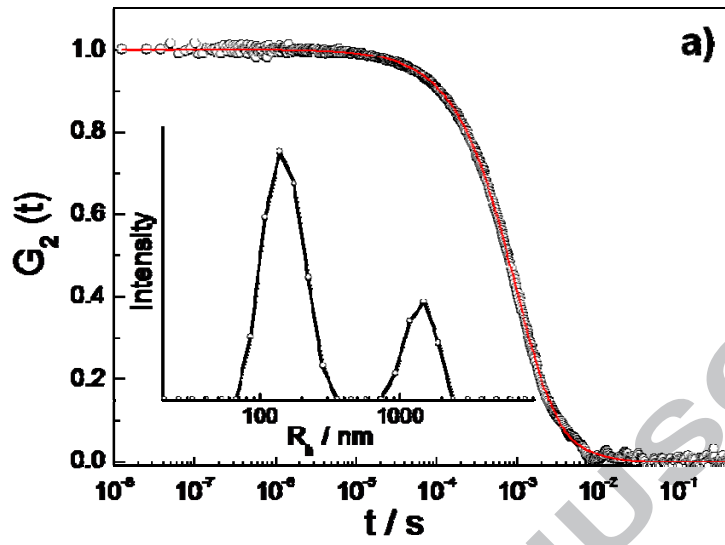
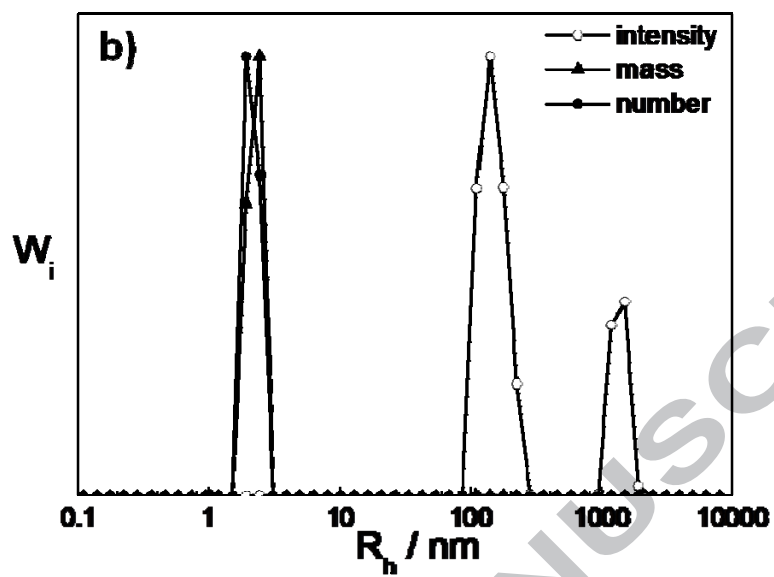
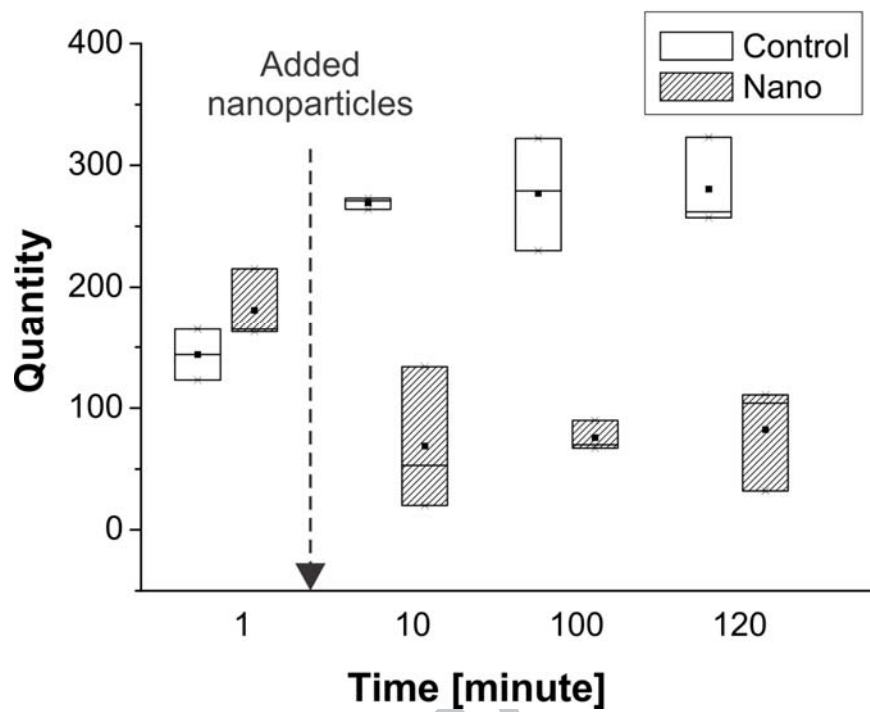
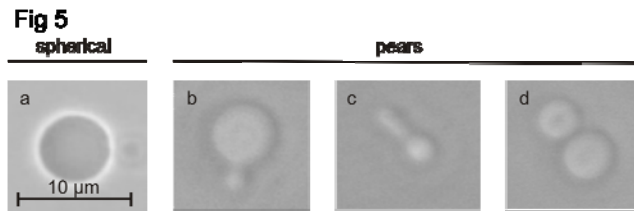


Fig 3b

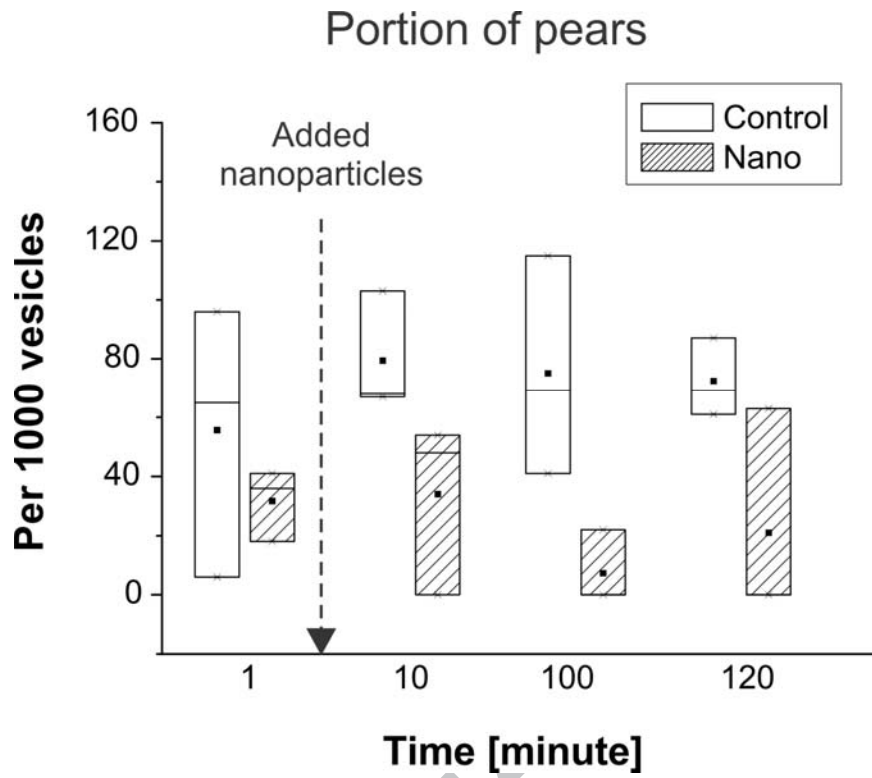


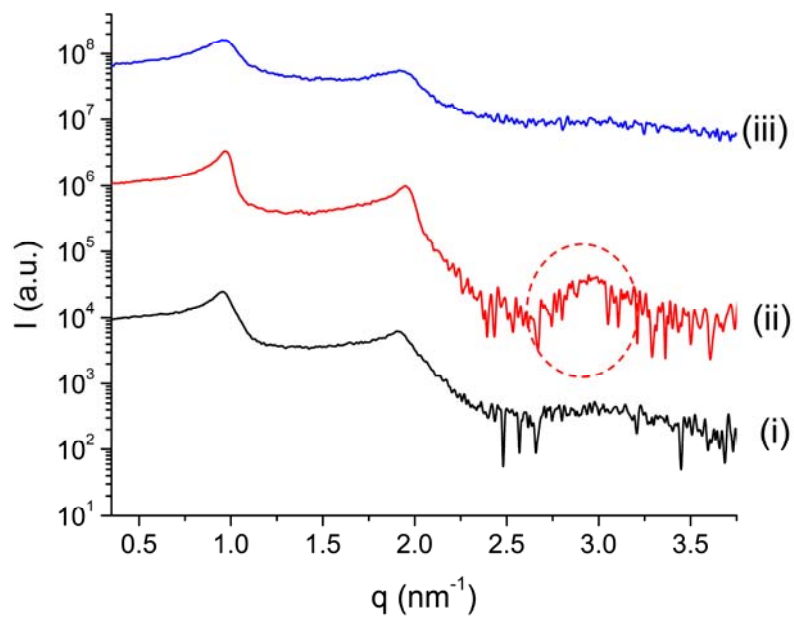
## C-60 exposed vesicle quantities





ACCEPTED MANUSCRIPT





ACCEPTED MANUSCRIPT

**Table caption:**

Table 1: Structural parameters of different POPC MLVs.

	<b>pure MLVs</b>	<b>MLVs with fullerene</b>	<b>MLVs with fullerene*</b>
$q_c$ ( $nm^{-1}$ )	0.949	0.962	0.954
$\Delta q_{exp}$ ( $nm^{-1}$ )	0.1360	0.0874	0.1797
$d$ (nm)	6.62	6.52	6.60
$N$	9	32	6

\*Additional treatment of 10 cycles of freeze and thaw (see sample preparation).